**Atmospheric
Chemistry
and Physics
Discussions**

Dust aerosol
radiative effect and
influence

L. Zhang et al.

Title Page

Abstract	Introduction
Conclusions	References
Tables	Figures

◄◄   ►►

◄   ►

Back   Close

Full Screen / Esc

Printer-friendly Version

Interactive Discussion

EGU

Dust aerosol radiative effect and influence on urban atmospheric boundary layer

L. Zhang[1,2], M. Chen[1,2], and L. Li[3]

[1]College of Atmospheric Sciences, Lanzhou University, Lanzhou, 730000, China
[2]Key Laboratory of Western China's Environmental Systems (Ministry of Education), Lanzhou University, Lanzhou, 730000, China
[3]Beijing Regional Climate Center, Beijing Meteorological Bureau, Beijing, 100089, China

Correspondence to: L. Zhang (zhanglei@lzu.edu.cn)

Abstract

An 1.5-level-closure and 3-D non-stationary atmospheric boundary layer (ABL) model and a radiation transfer model with the output of Weather Research and Forecast (WRF) Model and lidar AML-1 are employed to simulate the dust aerosol radiative effect and its influence on ABL in Beijing for the period of 23–26 January 2002 when a dust storm occurred. The simulation shows that daytime dust aerosol radiative effect heats up the ABL at the mean rate of about 0.68 K/h. The horizontal wind speed from ground to 900 m layer is also overall increased, and the value changes about 0.01 m/s at 14:00 LT near the ground. At night, the dust aerosol radiative effect cools the ABL at the mean rate of −0.21 K/h and the wind speed lowers down at about −0.19 m/s at 02:00 LT near the ground.

1 Introduction

As an important part of the earth's atmosphere, dust aerosol has caught an increasing attention. Going with dust storm, continuing floating dust weather influences people's life seriously and affects radiative budget at lower atmospheric layer. It is known that atmospheric aerosols reflect and absorb incoming solar radiation, thereby reduce the amount of sunlight available to the ground, which is called "direct" aerosol radiative effect. Aerosols also serve as cloud condensation nuclei (CCN) and change the albedo and microphysical properties of clouds, which is recognized as "indirect" aerosol radiative effect (Ramanathan et al., 2001).

There is a growing awareness of climate effect with mineral dust aerosol (McTainsh, 1989, 1990, 1998). Dust aerosol property such as physical characteristics, chemical composition, radiative effect and its transportation is gradually being opened out. The size distributions and chemical composition of particles are the key properties in determining the radiative effect of dust particles (Sokolik et al., 1998; Sokolik and Boon, 1999; Zhang and Wang et al., 2001). But the study on quantifying the dust aerosol influ-
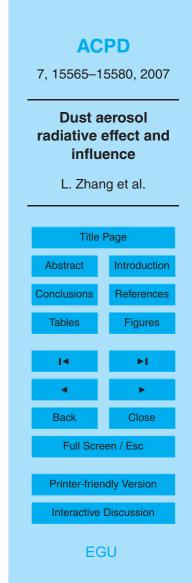
ence in a meteorological field is scarce and undetermined. The interaction of aerosols and infrared radiation often failed to be discussed. But it turns out to be an important mechanism in radiative forcing (Markowicz et al., 2003; Vogelmann et al., 2003). Alpert et al. (1998) indicate that dust aerosols tend to heat the lower atmosphere and thereby they are an important source of inaccuracies in numerical weather-prediction models. Li et al. (1998) simulate a super dust storm transport process and meteorological change, which shows that the dust aerosol tends to cool the atmosphere. The above-mentioned results reveal the complexity of dust aerosol radiative forcing, which mainly rests with refractive indices, single-scattering, albedo, asymmetry parameter and optical depth, while solar forcing is more sensitive to the changes of optical features than longwave forcing in general (Wang et al., 2006). Such a simulation of dust aerosol optical property by model may bring about some uncertain factors, therefore, observation data will be more useful and authentic. The paper intends to put the lidar data and data collected by National Centers of Environmental Prediction (NCEP) into the atmospheric model to simulate the dust aerosol radiative effect and its influence on urban ABL.

2 Data, model and verification

2.1 Data and model

NCEP $1° \times 1°$ reanalysis data are processed by the Weather Research and Forecasting (WRF) Model for simulation of the meteorological field over Beijing. The WRF model is a next-generation mesoscale numerical weather prediction system designed to serve both operational forecasting and atmospheric research. It can be employed to provide an initial meteorological field by featuring multiple dynamical cores, a 3-dimensional variation (3DVAR) data assimilation system, and a software architecture allowing for computational parallelism and system extensibility. WRF is suitable for a broad spectrum of applications across scales ranging from meters to thousands of kilometers.

The WRF model used here is Version 2.0 (Skamarock et al., 2005). It has major features as follows: 1) fully compressible equations, Euler nonhydrostatic with a run-time hydrostatic option available; 2) vertical coordinate: terrain-following hydrostatic-pressure with stretching vertical grids and a constant pressure surface model top; 3) horizontal grid: Arakawa C-grid staggering; 4) time integration: Time-split integration in a 3rd order Runge-Kutta scheme with smaller time step for acoustic and gravity-wave modes; 5) lateral boundary conditions: periodic, open, symmetric, and specified options available; 6) top boundary conditions: gravity wave absorbing (diffusion or Rayleigh damping). $w=0$ top boundary condition at constant pressure level. 7) bottom boundary conditions: physical or free-slip.

In the study the mobile lidar AML-1 measurement data of dust aerosol in Beijing (Yang et al., 2004) are also applied with the extinction coefficient detected by AML-1 in simulating dust aerosol radiative effect by a radiative transfer model (LOWTRAN 7).

LOWTRAN 7 is a low-resolution propagation model and a computer code for predicting atmospheric transmittance and background radiance from 0 to $50\,000\,\text{cm}^{-1}$ at a resolution of $20\,\text{cm}^{-1}$. Multiple scattering radiation is added to the model as well as new molecular band model parameters and new ozone and molecular oxygen absorption parameters for the UV. The model includes a wind dependent desert model, new cirrus cloud models, and new cloud and rain models. The code covers new and typical (geographical and seasonal) atmospheric models and updated aerosol models with user-derived values. An improved extra-terrestrial solar source function is further developed. Six modes of program execution are allowed with the new model and a computer code for a given slant path geometry. The code is capable of calculating atmospheric transmittance, atmospheric background radiance, single-scattered and earth-reflected solar and lunar radiance, direct solar irradiance, and multiple-scattered solar and thermal radiance.

The monochromatic radiation transfer equation of LOWTRAN 7 model is

$$\mu \cdot \frac{dI_{\upsilon}(l)}{d\tau} = I_{\upsilon}(\tau, \mu, \varphi) - J_{\upsilon}(\tau, \mu, \varphi) \tag{1}$$

where I_υ is the radiance, J_υ, the source function, τ, the vertical optical depth, μ, the cosine zenith angle and φ, the solar azimuth angle.

The vertical optical depth (τ) is composed of various mechanism contributions,

$$\tau = \int_z^\infty [\kappa_a(z) + \kappa_s(z) + \sigma_a(z) + \sigma_s(z)]dz \tag{2}$$

where κ_a, κ_s are the molecule absorption and scattering coefficient (km^{-1}) respectively; and σ_a, σ_s are the aerosol particle absorption and scattering coefficient (km^{-1}) respectively.

According to the Mie theory, the extinction coefficient is given by

$$\kappa_e(z) = \kappa_a(z) + \kappa_s(z) \tag{3}$$

$$\sigma_e(z) = \sigma_a(z) + \sigma_s(z) \tag{4}$$

which can be detected and retrieved by lidar data. In this way I_υ and the radiative flux (F) can also be calculated.

With the upward and downward radiative flux ($F^\uparrow$ and $F^\downarrow$) at different layers calculated by LOWTRAN 7, the net radiative flux $F_N(z)=F^\uparrow(z)-F^\downarrow(z)$ and the heating ratio can be worked out.

$$\left(\frac{\partial T}{\partial t}\right)_z = -\frac{1}{\rho \cdot c_p} \cdot \frac{F_N(z_2) - F_N(z_1)}{z_2 - z_1} = \frac{g}{c_p} \cdot \frac{F_N(z_2) - F_N(z_1)}{p(z_2) - p(z_1)} \tag{5}$$

where $p(z)$ is the atmospheric pressure at Layer z.

For the purpose of improving the modeling of WRF and simulating the radiative effect and the dynamic change caused by dust aerosol in Beijing, an 1.5-level-closure-3-D non-stationary ABL model was designed (Zhang, 2001). Input the heating ratio to the ABL model, the dust aerosol influence on the ABL can be simulated. In order to deal with the complex terrain, this ABL model is generally in the terrain-following ($z*$) coordinate system. The variables u, v, θ, and $w*$ are calculated by a staggered grid.

The calculation of advection term is made in the upstream scheme. As regards the vertical diffusion term an all-implicit time integration scheme is selected, while Euler integration scheme is applied to the rest of the terms. When the model is integrated in an almost-equilibrium state, the wind and temperature fields that are affected by dust aerosol can be obtained.

2.2 Model verification

The temperature, wind and pressure data used here were collected from 11 meteorological observing stations, Shunyi, Haidian, Miyun, Huairou, Tongzhou, Chaoyang, Changping, Mentougou, Guanxiangtai, Shijingshan and Fengtai in Beijing in September 2002.

The NCEP $1° \times 1°$ reanalysis data are taken into WRF as initial data. The simulation grid in WRF is designed as two-nests and three domains. The outside domain is 1500 km ×1500 km in the horizontal direction, the middle domain 400 km×400 km, the inside domain 80 km×80 km, and the spatial resolutions of the simulation domains are 50 km, 10 km and 2 km respectively. In the vertical direction, the simulation domain is divided into 33 layers, and the top layer pressure is 50 hPa. The center coordinate of the inner domain is 39.97° E and 116.37° N. The simulation started at 08:00 LT on 21 September 2002, ended at 00:00 on 23 September 2002, and the output file interval was set for one hour.

The ABL model is coupled with the WRF model with the same horizontal grid design and integral time. In the vertical direction, the domain is divided into 18 layers in terrain following coordinate and the height of the top layer is set to 1500 m. The model uses the WRF initial data as its input data and the WRF simulation result as its boundary condition to adjust its integral process. Through the re-integral process a new and better meteorological field can be obtained.

Figure 1 gives a comparison of surface temperature observation, the WRF and WRF-ABL simulations from 02:00 LT on 22 September to 20:00 LT on 23 September 2002, of Haidian and Changping respectively. The figures show that the simulation results are in

good agreement with the observed temperature. Moreover, the result of the WRF-ABL model is particularly closer to the observation than that of the WRF model, whereas the simulation of wind field is not as good as temperature. Though the shape is roughly similar to the observation, there are many differences in some part of the wind field. Nevertheless, the WRF-ABL model corresponds better with the observation than the single WRF model.

The study again makes an error analysis of the simulation result and the observation respectively (see Table 1) by using the following statistic parameters (Fox, 1981).

The error (A_d) between observation (A_{obs}) and simulation (A) is given by

$$A_d = A_{obs} - A \tag{6}$$

The temporal average or spacial average (M_d) of A_d is

$$M_d = \sum A_d/N \tag{7}$$

The ratio error (e) between A_{obs} and A is described as

$$e = 2(A - A_{obs})/(A + A_{obs}) \tag{8}$$

The temporal average or spacial average (e_m) of e is

$$e_m = \sum e/N \tag{9}$$

These parameters show the difference between the simulation value and the observation value, which can, therefore, reflect the modeling capability of the two models.

Table 1 lists the error and ratio error of the surface temperature at 02:00 LT and 14:00 LT on 23 September 2002 in 11 ground stations. It shows clearly that the errors of the WRF-ABL model are all smaller than that of the WRF model. Thus the WRF-ABL model is verified better in the simulation.
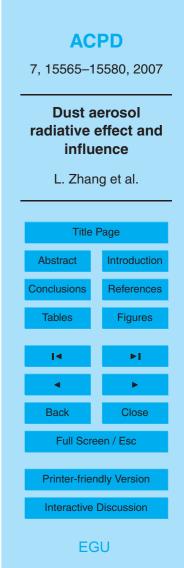
EGU

3   Dust aerosol radiative effect and its influence on ABL

24 January 2002 is a typical day for simulation when a dust storm struck Beijing. During the dust storm, the wind speed and temperature changed greatly. Figure 2 shows the extinction coefficient profile from the AML-1 lidar measurement at 10:00 LT on 24 January (Yang et al., 2004). The model integral started at 08:00 LT on 23 January. In order to calculate the response of ABL to the dust aerosol radiative forcing, two schemes are designed: one is an ordinary scheme without aerosol radiative effect, and the other a radiative scheme with aerosol radiative effect. The difference of the two models demonstrates the ABL response to the dust aerosol radiative forcing.

3.1   Daytime ABL response to the dust aerosol radiative effect

During these dust floating days, the steady meteorological fields held back the pervasion of the regional anthropogenic pollutant aerosol which brought about two kinds of aerosols, and changed the optical property of floating dust aerosol. The change enhances the dust aerosol absorbing property, which shows that dust aerosol absorbs the short wave radiation and heats up the atmosphere at daytime. The effect starts at sunrise, continues all the daytime, and ends at sundown. In the afternoon, the calefacient effect will reach the highest value at 14:00 LT. Figure 3 presents the results simulated by two different schemes. Figure 3a is a temperature profile that shows the heating effect of dust aerosol is bigger at lower layer (1.07 K/h near the ground) than at higher layer (0.28 K/h on 900 m layer), and the average temperature increases at about 0.68 K an hour. The great calefacient effect also affects the ABL structure. Because the temperature rises faster at lower layer than at higher layer, it intensifies convection, weakens stability and changes the horizontal velocity in ABL. Figure 3b is a horizontal velocity profile that indicates the velocity steadily goes up from the ground to 900 m layer. The velocity variation is about 0.01 m/s at 14:00 LT near the ground.

3.2 Nighttime ABL response to the dust aerosol radiative effect

Dust aerosol may change the long wave radiative effect and accordingly, the drop of atmospheric temperature occurs with dust floating at night. Figure 4a tells the difference of temperature with aerosol effect and without aerosol effect at 02:00 LT on 24 January 2002. The temperature near the ground decreases at 0.09 K an hour, which is much lower than that at higher layer (900 m) where the temperature drops at 0.47 K an hour. The average value from the ground to 900 m layer is about −0.21 K/h. At the same time, the changed temperature regulates the wind field (see Fig. 4b) and affects the stability of ABL. The result shows that the horizontal velocity from the ground to 900 m layer tends to drop at night, the variation is about −0.19 m/s at 02:00 LT near the ground.
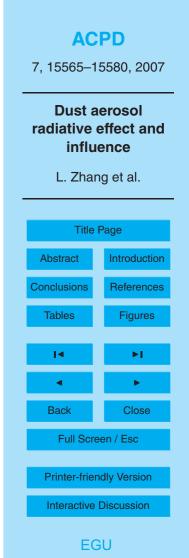
4 Discussion and conclusion

An integrated model, coupled with the WRF model, an ABL model and an atmospheric radiative transfer model, is used to simulate the temperature and wind speed fields in Beijing. The simulation worked out by the integrated model can present a better meteorological field than by a single WRF model.

Through lidar measurements we can get the distribution of real-time dust aerosol extinction coefficient and other optical parameters, which can be used as input data of the radiative transfer model to simulate temperature variation.

At daytime, the dust aerosol radiative effect will raise the low atmosphere temperature at about 0.68 K an hour. The wind speed from the ground to 900 m layer tends to increase. Near the ground it rises at about 0.01 m/s at 14:00 LT, while at higher layer the speed increase is faster than at lower layer.

Because of the dust aerosol radiative effect the atmospheric temperature tends to drop from the ground to 900 m layer at night with an average value of −0.21 K/h. Again the changed temperature modifies the wind field and affects the stability of ABL. The

horizontal velocity from the ground to 900 m layer often drops at night. It slows down at about −0.19 m/s at 02:00 LT near the ground

References

Alpert, P., Kaufman, Y. J., Shay-El, Y., Tanre, D., da Silva, A., Schubert, S., and Joseph, J. H.: Quantification of dust-forced heating of the lower troposphere, Nature, 395, 367–370, 1998.

Fox, D. G.: Judging air quality model performance, Bull. Am. Meteorol. Soc., 62(5), 599–609, 1981.

Li, X. S., Zhou, J. Q., Li, Z., Fang, X. M., He, Z. S., and Parungo, F.: A Numerical Simulation of "5.5" Super-Duststorm in Northern China, Adv. Atmos. Sci., 15(1), 63–73, 1998.

Markowicz K. M., Flatau, P. J., Vogelmann, A. M., Quinn, P. K., and Welton, E. J.: Clear-sky infrared aerosol radiative forcing at the surface and the top of the atmosphere, Q. J. R. Meteorol. Soc., 129, 2927–2947, 2003.

McTainsh, G. H., Burges, R. C., and Pitblado, J. R.: Aridity drought and dust storms in Australia (1960–1984), J. Arid Environ., 16, 11–22, 1989.

McTainsh, G. H., Lynch, A. W., and Burgess, R. C.: Wind erosion in eastern Australia, Australian J. Soil Res., 28, 323–339, 1990.

McTainsh, G. H., Lynch, A. W., and Tews, E. K.: Climatic controls upon dust storm occurrence in eastern Australia, J. Arid Environ., 39, 457–466, 1998.

Ramanathan, V., Crutzen, P. J., Kiehl, J. T., and Rosenfeld, D.: Aerosols, Climate, and the Hydrological Cycle, Science, 294, 2119–2124, 2001.

Skamarock, W. C., Klemp, J. B., Dudhia, J., Gill, D. O., Barker, D. M., Wang, W., and Powers, J. G.: A Description of the Advanced Research WRF Version 2. National Center for Atmospheric Research, 88pp, http://www.mmm.ucar.edu/wrf/users/docs/arw_v2.pdf, 2005.

Sokolik, I. N., Toon, O. B., and Bergstrom, R. W.: Modeling the radiative characteristics of airborne mineral aerosols at infrared wavelength, J. Geophys. Res., 103, 8813–8826, 1998.

Sokolik, I. N. and Toon, O. B.: Incorporation of mineralogical composition into models of radiative properties of mineral aerosol from UV to IR wavelength, J. Geophys. Res., 104, 9423–9444, 1999.

EGU

Vogelmann, A. M., Flatau, P. J., Szczodrak, M., Markowicz, K. M., and Minnett, P. J.: Observation of large aerosol infrared forcing at the surface, Geophys. Res. Lett., 30(12), 1655, doi:10.1029/2002GL016829, 2003.

Wang, H., Shi, G. Y., Li, S. Y., Li, W., Wang, B., and Huang, Y. B.: The Impacts of Optical Properties on Radiative Forcing Due to Dust Aerosol, Adv. Atmos. Sci., 23(3), 431–441, 2006.

Wang, M. X. and Zhang, R. J.: Frontier of Atmospheric Aerosols Researches, Climatic and Environmenta1 Research, 6(1), 119–124, 2001.

Yang, L. J., Zhang, Y. C., Liu, X. Q., et al.: Optical Properties of Aerosol Detected by Mobile Lidar System, Chinese Journal of Quantum Electronics, 21(1), 88–91, 2004.

Zhang, L.: A study of interaction of urban atmospheric aerosol and boundary layer, Ph. D. dissertation, Lanzhou University, 96 pp., 2001.
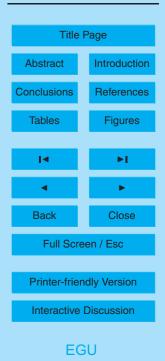
Zhang, R. J., Wang, M. X., and Fu, J. Z.: Preliminary research on the size distribution of aerosols in Beijing, Adv. Atmos. Sci., 18(2), 225–230, 2001.

Title Page

Abstract | Introduction

Conclusions | References

Tables | Figures

◄ | ►

◄ | ►

Back | Close

Full Screen / Esc

Printer-friendly Version

Interactive Discussion

EGU

Table 1. Temperature simulation error analysis.

09-23-2002	02:00				14:00			
	Boundary Model		WRF Model		Boundary Model		WRF Model	
Station	A_d	e	A_d	e	A_d	e	A_d	e
Shunyi	1.16	−0.25	−2.2	0.16	0.47	0.02	1.04	−0.03
Haidian	0.2	−0.07	−1.03	0.06	0.32	0.05	1.9	−0.06
Miyun	−0.13	−0.05	−0.84	0.06	0.76	−0.08	−1.71	0.05
Huairou	−0.96	−0.03	−1.41	0.10	−0.54	0.04	0.57	−0.02
Tongzhou	0.39	0.03	1.09	−0.05	0.64	0.03	1.44	−0.05
Chaoyang	0.91	−0.10	−0.69	0.04	0.54	0.01	0.89	−0.03
Changpin	0.8	−0.09	−0.9	0.05	1.2	0.01	1.6	−0.05
Mentougou	0.66	−0.08	−0.8	0.04	0.11	0.02	0.82	−0.03
Guanxiangtai	0.65	−0.04	−0.05	0.00	0.86	−0.01	0.57	−0.02
Shijingshan	0.12	−0.09	−1.39	0.08	1.13	0.00	1.23	−0.04
Fengtai	1.06	−0.12	−1.24	0.06	0.81	0.02	1.38	−0.05
Mean	0.442	−0.08	−0.86	0.05	0.573	0.01	0.885	−0.03

* A_d error of the surface temperature.
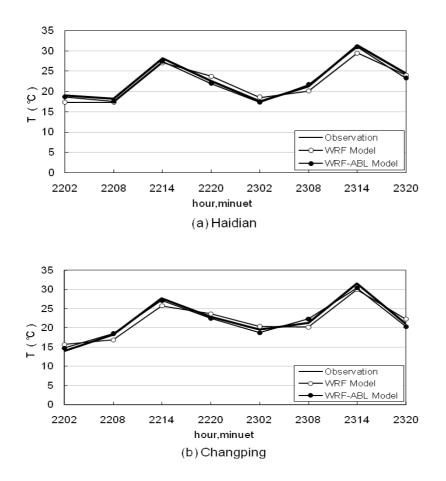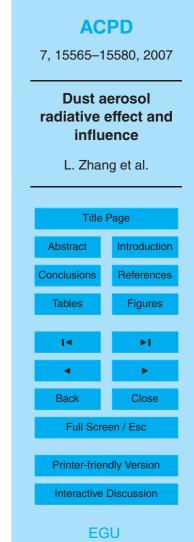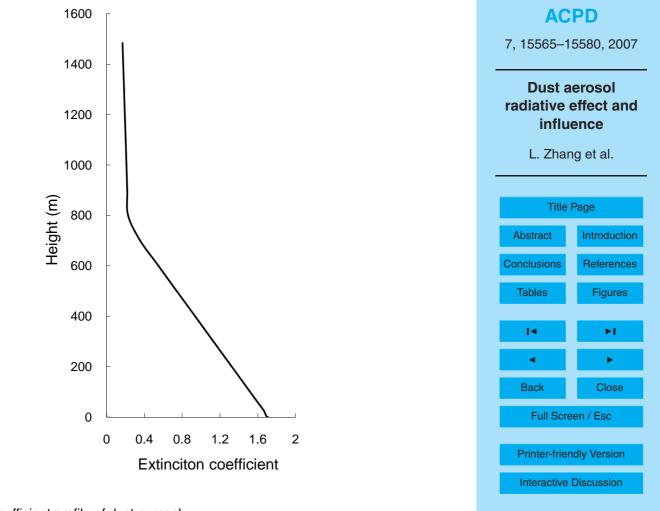* e ratio error of the surface temperature.

Fig. 1. Surface temperature of observation, WRF model and WRF-ABL model in Haidian and Changping from 02:00 LT 22 September to 20:00 LT 23 September 2002.

Fig. 2. Extinction coefficient profile of dust aerosol.
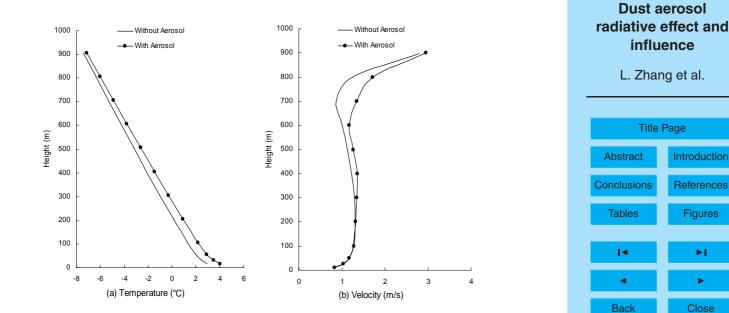
Title Page

Abstract · Introduction

Conclusions · References

Tables · Figures

◄◄ · ►►

◄ · ►

Back · Close

Full Screen / Esc

Printer-friendly Version

Interactive Discussion

EGU

Fig. 3. Differences of temperature and velocity at 14:00 LT, 24 January 2002.

Fig. 4. Differences of temperature and velocity at 02:00 LT, 24 January 2002.

Title Page

Abstract | Introduction

Conclusions | References

Tables | Figures

◄ | ►

◄ | ►

Back | Close

Full Screen / Esc

Printer-friendly Version

Interactive Discussion

EGU